Surface Complexation of Carboxylate Adheres *Cryptosporidium parvum* Oocysts to the Hematite−Water Interface

XIAODONG GAO,[†] DAVID W. METGE,[‡] CHITTARANJAN RAY,[§] RONALD W. HARVEY,[‡] AND JON CHOROVER[†,*]

Department of Soil, Water and Environmental Science, University of Arizona, Tucson, Arizona 85721, Water Resources Division, United States Geological Survey, Boulder, Colorado 80303, and Department of Civil and Environmental Engineering, University of Hawaii at Manoa, Honolulu, Hawaii 96822

Received May 6, 2009. Revised manuscript received August 16, 2009. Accepted August 20, 2009.

The interaction of viable *Cryptosporidium parvum* öocysts at the hematite (α-Fe_2O_3)−water interface was examined over a wide range in solution chemistry using in situ attenuated total reflectance Fourier transform infrared (ATR-FTIR) spectroscopy. Spectra for hematite-sorbed öocysts showed distinct changes in carboxylate group vibrations relative to spectra obtained in the absence of hematite, indicative of direct chemical bonding between carboxylate groups and Fe metal centers of the hematite surface. The data also indicate that complexation modes vary with solution chemistry. In NaCl solution, öocysts are bound to hematite via monodentate and binuclear bidentate complexes. The former predominates at low pH, whereas the latter becomes increasingly prevalent with increasing pH. In a $CaCl_2$ solution, only binuclear bidentate complexes are observed. When solution pH is above the point of zero net proton charge (PZNPC) of hematite, öocyst surface carboxylate groups are bound to the mineral surface via outer-sphere complexes in both electrolyte solutions.

Introduction

Cryptosporidium parvum is a protozoan pathogen that infects a wide range of hosts, including humans, livestock, and wildlife. The pathogen exists as a dormant öocyst in the environment, which is resistant to various environmental stresses, including freezing, desiccation, and chlorination. Once ingested, however, the öocysts exist in the small intestine, leading to the diarrheal disease Cryptosporidiosis, which is potentially lethal, particularly for immuno-suppressed individuals (*1*).

The environmental fate and transport of öocysts have been widely studied in the past decade. However, most of the prior work has focused on quantifying electrostatic and steric effects on öocyst adhesion to model minerals or natural soil particles (*2*−*8*). Long-range electrostatic forces can promote adhesion when öocysts and substrate surfaces are oppositely charged and diminish adhesion when they are of like charge. Short-range steric effects have been reported to inhibit öocyst adhesion to silica particles because of unfavorable surface polymer overlap (*3, 5*−*7*). In a previous spectroscopic study, we found that öocyst surfaces are populated by a complex mixture of biomacromolecules with amide, carboxylate, phosphate, and carbohydrate functionalities, and that adhesion to the ZnSe surface was significantly affected by changes in the molecular structure of these surface biomacromolecules that accompany alterations in solution chemistry (*9*). In addition, for adhesion to the ZnSe surface, these effects were consistent with electrostatic and steric interaction mechanisms (*9*).

In addition to electrostatic and steric interactions, biomolecular functional groups may also serve as reactive sites for direct chemical bonding to hydroxylated mineral surfaces (*10*). If it occurs, such bonding may play an important role in mediating the fate and transport of pathogenic cells in subsurface environments. Direct bonding of phosphate and phosphodiester groups to surface Fe metal centers was observed during adhesion of extracellular polymeric substances (EPS) (*10, 11*) and intact bacterial cells (*12*) to Fe (oxyhydr)oxide surfaces. In addition, inner-sphere complexation of carboxylate groups with Fe was observed during adhesion of *Pseudomonas putida* to hematite (*13*). No comparable studies have been conducted for pathogenic *Cryptosporidium* öocysts.

Ferric and Al oxyhydroxides are abundant, particularly in highly weathered variable charge soils such as those found in the humid tropics and southeastern United States. Even in less weathered soils and aquifer sediments such oxides often coat the surface of quartz or feldspar grains, conferring net positive surface charge at circumneutral pH (*14*). Several column transport (*4, 15*) and batch adsorption experiments (*16*) with microbial cells have demonstrated that Fe oxide coatings substantially diminish cell transport in porous media by increasing surface adhesion. Hematite, one of the most abundant Fe oxide phases in weathered soils and one that often occurs naturally in nanoparticulate form (*17*), was therefore chosen as a model mineral in the present work to elucidate the likely adhesion mechanisms of öocysts in Fe-rich soils.

ATR-FTIR spectroscopy is a surface-sensitive technique that can provide molecular-scale information on interfacial reactions involving microbial cells in aqueous suspension (*9, 11, 12, 18*). In this study, ATR-FTIR was employed to investigate the adhesion of viable *C. parvum* öocysts to nanoparticulate α-Fe_2O_3 surface coatings affected by aqueous solution chemistry. The primary objective was to elucidate the role of surface biomacromolecules in mediating adhesion and, therefore, to assess their effect on controlling pathogen transport in the subsurface.

Materials and Methods

Öocyst Preparation. All *C. parvum* öocysts used in this study were obtained from the Sterling Parasitology Laboratory at the University of Arizona. The öocysts were shed from a calf infected with the Iowa Isolate of *C. parvum* at the National Animal Disease Center in Ames, IA. Öocysts were purified by discontinuous sucrose and cesium chloride (CsCl) centrifugation gradients, then stored at 4 °C in an antibiotic solution containing 0.01% Tween 20, 111 U penicillin, 111 U streptomycin, and 100 μg mL^{-1} of gentamicin. Prior to performing the infrared spectroscopy experiments, öocysts were washed and resuspended to give a final cell concentration of 2×10^7

* Corresponding author phone: 520-626-5635; fax: 520-621-1647; e-mail: chorover@cals.arizona.edu.
† University of Arizona.
‡ United States Geological Survey.
§ University of Hawaii at Manoa.

10.1021/es901346z CCC: $40.75
Published on Web 09/01/2009

mL^{-1} in a NaCl or $CaCl_2$ background electrolyte at an ionic strength of 10 mM, corresponding to concentrations of 10 and 3.3 mM for NaCl and $CaCl_2$, respectively. The suspension pH was adjusted to 3.0, 4.5, 6.0, 7.5, and 9.0 using HCl or NaOH [or $Ca(OH)_2$ in the case of a $CaCl_2$ background electrolyte] at the same ionic strength. A detailed description of the method is given in Gao and Chorover (*9*).

Hematite Synthesis and Characterization. Colloidal hematite was synthesized following the methods of Schwertmann and Cornell (*19*). One hundred milliliters of 1 M $Fe(NO_3)_3 \cdot 9H_2O$ solution were added dropwise to 1 L of boiling Barnstead Nanopure (BNP) water during vigorous stirring. The suspension was allowed to cool to room temperature before being transferred into dialysis tubes (Spectra/Por 7 1000 MWCO) and was dialyzed against BNP water (replaced twice daily) with pH adjusted to 4.0 using a 0.1 M HNO_3 solution. Dialysis was considered complete when pH stabilized at 4.0 (about 2 weeks), at which time the colloidal suspension was transferred to a polyethylene bottle and stored at 4 °C. The concentration of hematite was determined by freeze-drying an aliquot of the colloidal suspension and measuring the dry mass.

Mineralogical composition and purity for synthetic hematite was confirmed using synchrotron X-ray diffraction (XRD) conducted at the Stanford Synchrotron Radiation Lightsource on beamline 11−3 (Figure S1 of the Supporting Information). Transmission electron microscopy (Philips FEI CM12 STEM) showed roughly spherical particles, 10−20 nm in diameter (Figure S2 of the Supporting Information). The electrophoretic mobility of hematite colloids, measured at a solid concentration of 0.1 g L^{-1} in 1 mM $NaNO_3$ over the pH range of 4.0−9.0 adjusted using 1 or 10 mM NaOH or HCl, (Brookhaven Instruments ZetaPALS, NY) showed a point of zero charge at pH 7.7−7.8 (Figure S3 of the Supporting Information).

Hematite Coating of IRE Surface. To achieve a uniform, thin layer of hematite film on the ZnSe internal reflection element (IRE) surface of the ATR cell, we first diluted the α-Fe_2O_3 colloidal suspension (6.6 g L^{-1}) to 3.3 g L^{-1} with 100% ethanol, and 500 uL of the diluted suspension were evenly deposited onto the IRE surface and allowed to dry in a vacuum oven (10 mmHg) overnight at room temperature. The addition of ethanol to the suspension improves particle adhesion to the ATR crystal and yields more uniform coating (*20*). After drying, the hematite film was gently rinsed with BNP water to remove loosely adhered particles. A new hematite coating was prepared for each experiment, and spectra of dry oxide films were acquired each time to determine consistency of coating.

ATR-FTIR Spectroscopy Analysis. A Magna-IR 560 Nicolet spectrometer (Madison, WI) equipped with a CsI beam splitter and a DTGS detector was used to collect all ATR-FTIR spectra. Spectra were obtained using a 45° trough-style sample holder with a zinc selenide (ZnSe) internal reflection element (56 mm × 10 mm × 3 mm) (PIKE Technologies, Inc.) yielding nine internal reflections. For each solution chemistry condition, an aliquot of the öocyst suspension (∼500 μL) was applied directly to the uncoated or hematite-coated ZnSe IRE by pipet. To examine the temporal dependence of surface interaction, we collected spectra as a function of time (0, 15, 30, 60, 120, 180, and 240 min after sample introduction) at room temperature. A volatile liquid cover was used to limit solution evaporation during the measurements.

A total of 400 scans with a spectral resolution at 4 cm^{-1} were collected and averaged over the spectral range of 4000−800 cm^{-1} for each sample. A final sample spectrum was obtained by subtracting the appropriate background spectrum (e.g., öocyst-free electrolyte on ZnSe IRE or α-Fe_2O_3-coated IRE) from the spectrum of the öocyst suspension.

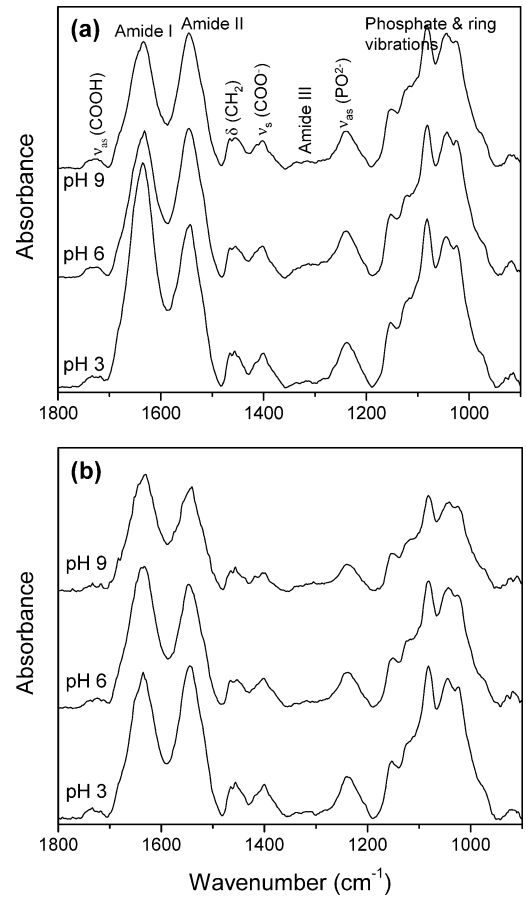

FIGURE 1. ATR-FTIR spectra of viable öocyst suspension on ZnSe IRE as a function of pH in (a) 10 mM NaCl solutions and (b) 10 mM $CaCl_2$ solutions.

The dry, clean 45° ZnSe crystal was consistently used for background correction. The spectrometer was continuously purged with CO_2 free air to eliminate CO_2 absorption. Data collection and spectral processing, including subtraction and baseline correction, were performed using the OMNIC program (Thermo Nicolet Co.). Because baseline slope was not linear across the entire spectral region, multipoint baseline fits were performed for each spectrum to yield a flat baseline. Quantitative Lorentzian peak fitting was performed using GRAMS/AI software (Thermo Electron Corp.).

Results and Discussion

ATR-FTIR Spectra of Öocysts on ZnSe IRE Surface. ATR-FTIR spectra of viable öocysts introduced to the uncoated ZnSe IRE surface are shown as a function of pH in NaCl (Figure 1a) and $CaCl_2$ (Figure 1b) background electrolytes. The spectra show only a small variation with solution pH and ion composition and are very similar overall. The only difference observed is that öocyst adhesion to the IRE as measured by the absorbance of the amide II band following deconvolution (*9*) increased with decreasing pH. The spectra are dominated by several distinct bands corresponding to amides (1635, 1542, and 1337−1313 cm^{-1} for amide I, amide II, and amide III, respectively), carboxylate (COO^- at 1400 cm^{-1}), phosphate (1247 cm^{-1}), and polysaccharide functional groups (C−O−C, C−C, 1150−950 cm^{-1}). The small peak at ∼1720 cm^{-1} is a combination of two bands corresponding to the stretching of protonated carboxyl groups (COOH) and C═O of ester groups (Table S1 of the Supporting Information). Our prior study indicated that adhesion to the ZnSe surface is dominated by a combination of electrostatic and electrosteric forces (*9*).

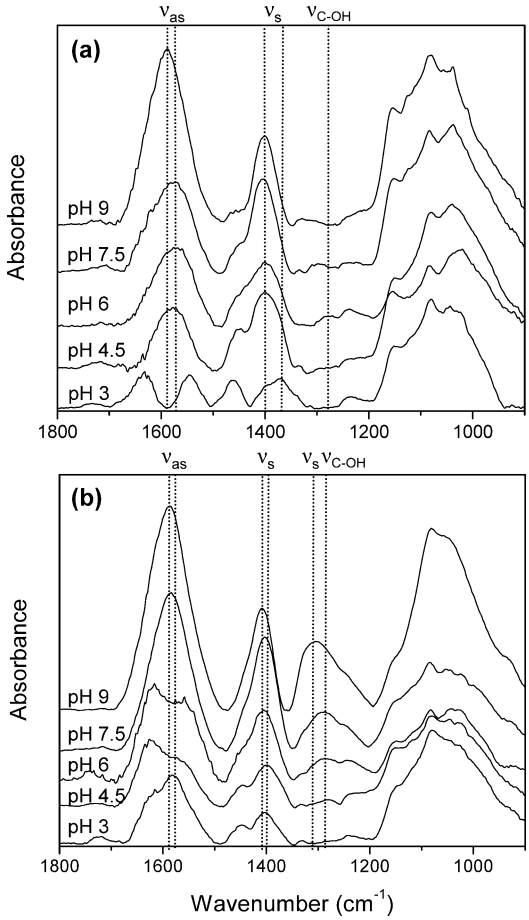

FIGURE 2. ATR-FTIR spectra of viable öocyst suspension on a hematite surface as a function of pH in (a) 10 mM NaCl solutions and (b) 10 mM $CaCl_2$ solutions.

ATR-FTIR Spectra of Öocysts on Hematite Surface. Spectra of the öocyst suspensions introduced to the hematite-coated surface in 10 mM NaCl solutions are shown in Figure 2a. The major changes resulting from interaction with hematite occur in the carboxylate stretching regions, including protonation and deprotonation of carboxyl groups. Carboxylate group absorbances increased substantially with increasing pH relative to other bands (e.g., polysaccharides and amides) in the spectra. Carboxylate group assignments are summarized in Table 1. The only carboxylate band observed for öocysts on ZnSe is the symmetric stretching at 1400 cm^{-1}, the appearance of which is independent of pH and ionic composition in our experiments (Figure 1). Conversely, in the presence of hematite, carboxylate group vibrations are very sensitive to changes in solution pH, consistent with their known sensitivity to changes in protonation state and local coordination (*21*). The infrared spectra of protonated carboxyl (COOH) are characterized by strong absorbance at 1750−1700 and 1300−1200 cm^{-1} corresponding to the C═O and C−OH bonds, whereas the deprotonated carboxylate (COO^-) exhibits strong asymmetric (ν_{as}) and relatively strong symmetric (ν_s) stretching at 1650−1510 and 1400−1280 cm^{-1}, respectively (*22*). The precise frequencies depend on neighboring functional groups (*23*).

Similar to the spectra for the uncoated IRE, a small band at ∼1730 cm^{-1} was observed across the experimental pH range that could potentially be assigned to asymmetric stretching of protonated carboxyl moieties (Figure 2a). However, stretching of ester C═O groups also occurs at ∼1725 cm^{-1}. Because the intensity of the band is almost independent of pH, it is likely that ester group vibrations contribute significantly. Furthermore, no other bands reflecting protonated carboxylic groups (e.g., ν_{C-OH}) were observed in the spectra at pH 3, suggesting that the öocyst surface carboxylic groups are mostly deprotonated even at pH 3. Because polysaccharides and proteins are the major surface components of öocysts (*9*), a negative öocyst surface charge originates principally from the ionization of acidic groups in the amino acids with pK_a values of ranging from pH 1.71 to 3.0 (*24*). Hence, such carboxyl groups are strongly acidic and largely dissociated even at the lower pH limit of our experiment (pH 3). Likewise, Jiang et al. (*18*) reported that the band at ∼1720 cm^{-1} corresponding to the stretching of C═O in COOH groups on bacterial surfaces emerges only at pH ≤ 2. Furthermore, carboxyl groups are observed to be deprotonated upon adsorption to hematite even below the corresponding pK_a for bulk solution (*21, 25*).

The asymmetric stretching of COO^- is masked by the large amide group absorbance at pH 3. However, the band at 1577 cm^{-1} corresponding to ν_{as} (COO^-) increased dramatically and became the dominant band in the "amide" range above pH 4.5. In addition, the band frequency shifts to a higher wavenumber from 1577 to 1587 cm^{-1} at pH 9.

The most distinct changes in the spectra of hematite-adsorbed öocysts occur in the symmetric stretching region of carboxylate (1400−1300 cm^{-1}). The band intensity at ∼1400 cm^{-1} corresponding to ν_s (COO^-) grows progressively with pH relative to the δ (CH_2) band at 1457 cm^{-1}. Two distinct bands in this region at 1400 and 1370 cm^{-1} were observed at pH 3. Peak shifts or splitting in the ATR-FTIR spectra are often resulted from the formation of carboxylate-metal inner-sphere complexes (*13, 17, 20−22*). Therefore, the splitting of the symmetric stretching band indicates the formation of one or more inner-sphere complexes between Fe oxide and carboxylic groups (*21*). The complexation mode represented by the band at 1370 cm^{-1} dominates at pH 3. With increasing pH, the intensity ratio between the bands at 1400 and 1370 cm^{-1} increases. The band at 1370 cm^{-1} becomes a shoulder at pH 4.5 and 6 and disappears at pH 7.5 and 9 (Figure S4 of the Supporting Information). This change indicates that the binding mechanism between hematite and öocysts gradually shifts from one type of complexation mode to another with increasing pH.

A new band at ∼ 1290 cm^{-1} emerges in the spectra at pH 4.5, 6, and 7.5 (Figures 2 and 4). The frequency of the band matches the stretching of ν_{C-OH} (COOH) reported in the literature (*21, 22*), but the pH range where it occurs exceeds the pK_a of carboxylic acid. A similar finding was reported for bacterial cell adhesion to Fe oxide (*12*), where it was suggested that the band results from sorption-induced protonation of carboxylate. That is, although the pH range from 4.5 to 7.5 is above the pK_a of öocyst surface carboxylate groups, it is below the PZNPC of hematite. The hydroxyl groups at the mineral surface may, therefore, form H-bridges with öocyst surface carboxyls. Below pH 3 or above pH 9, the two surfaces carry the same charge sign, hindering the formation of such H-bridges.

Effects of Cation type. Figure 2b shows the spectra of a viable öocyst suspension introduced to the hematite surface in 10 mM $CaCl_2$ across a range of pH. The spectra show similar features to those obtained in NaCl solutions, especially in terms of increasing absorbance of the asymmetric and symmetric carboxylate stretching with pH. However, there are also some important differences. First, the carboxylate absorbances are stronger in presence of Ca^{2+} relative to Na^+ at pH 3 (Figure 2a), particularly the asymmetric stretch. Second, the symmetric stretch contains only one band at 1400 cm^{-1}, consistent with a single mode of surface complexation. Third, at pH 9, relative to the Na^+ case, the position of ν_s (COO^-) is shifted to slightly higher wavenumber (from 1400 to 1409 cm^{-1}, Figure 2b and Figure 4). Fourth,

TABLE 1. Experimental Frequencies (cm^{-1}) and Assignments of Carboxylate Groups Observed in ATR-FTIR Spectra of Oocysts at a Hematite Surface

assignment	NaCl background electrolyte (pH)					$CaCl_2$ background electrolyte (pH)				
	3.0	4.5	6.0	7.5	9.0	3.0	4.5	6.0	7.5	9.0
ν_{as} (COO^-)		1577	1577	1577	1587	1583	1583	1583	1585	1587
ν_s (COO^-)	1400 1370	1400 1379	1400	1403	1400	1400	1400	1400	1405	1409
					1331	1331	1331			1305
ν_s (C−OH)		1290	1297	1280			1281	1286	1286	

carboxylate absorbances are much stronger in presence of Ca^{2+} relative to Na^+ at pH 9. Finally, two additional bands were observed in the Ca system spectra. The peak at ~1305 cm^{-1} at pH 9 has been previously observed for polycarboxylic acids such as oxalic acid (*20, 22*) and maleic acid (*25*) and has been attributed to the symmetric stretching of COO^- groups. An additional small peak at ~1330 cm^{-1} was observed in the spectra at low pH values (Figure 4f,g). On the basis of its frequency, it is tentatively assigned as another carboxylate symmetric stretching vibration.

Fe−Carboxylate Outer-sphere Complexation. The differences in spectra between adsorbed species and aqueous species, including peak emergence, splitting, and changes in relative intensities between ν_s (COO^-) and ν_{as} (COO^-), can be used to distinguish the structure of inner-sphere and outer-sphere surface complexes (*17*). Surface complexation of low molecular weight (LMW) carboxylic acids on various hydroxylated mineral surfaces, including α-Fe_2O_3 (*17, 20, 21, 25*), α- and γ-Al_2O_3 (*22, 23, 26*), and TiO_2 (*27*), has been observed using ATR-FTIR. These studies indicate either outer-sphere or inner-sphere coordination depending on ligand structure, mineral surface type, and solution chemistry (e.g., pH and surface loading).

The spectra of öocyst suspensions in the presence of hematite at pH 9 for NaCl and $CaCl_2$ background electrolytes (Figure 2a,b) are similar to those of the aqueous species of LMW carboxylic acids (*21, 22, 25*). Such spectra contain strong asymmetric and weaker symmetric stretching peaks. In addition, hematite and öocysts are negatively charged at this pH, which diminishes the tendency for inner-sphere complexation via ligand exchange (*28*). Therefore, we propose that at pH 9, öocysts are bound to the hematite surface via outer-sphere complexation. Nonetheless, öocyst spectra at pH 9 in the presence and absence of hematite are distinctly different (compare Figure 2 to Figure 1); COO^- bands dominate the spectra from 1700−1300 cm^{-1} when hematite is present, indicating significant öocyst−hematite interaction even at pH 9 when both surfaces are negatively charged. The ZnSe IRE is hydrophobic relative to hematite (*29*) such that the latter may exhibit a higher affinity for carboxylate. In addition, the nanoparticulate hematite used here presents a very high interfacial area for öocyst interaction.

Furthermore, compared to the öocyst pH 9 NaCl spectrum (Figure 2a), that for $CaCl_2$ (Figure 2b) shows an additional symmetrical COO^- stretching peak at 1305 cm^{-1}. The peak at 1400 cm^{-1} is shifted to a higher wavenumber (from 1400 to 1409 cm^{-1}), and the overall spectral absorbances are much higher in $CaCl_2$. These differences are consistent with cation-bridging, where bivalent Ca^{2+} more effectively than Na^+ bridges the negatively charged hematite and öocyst surfaces. This bridging interaction increases öocyst adhesion to the hematite surface and changes the coordination environment of carboxylate groups, as indicated by the emergence of the peak at 1305 cm^{-1} and shift of the peak at 1400 to 1409 cm^{-1}.

Fe−Carboxylate Inner-sphere Complexation. For studies with simple carboxylic acids, it is common practice to use the IR spectra of aqueous species as a reference to determine the complexation mode of adsorbed species (*17, 21, 25*). Surface coordination is assigned on the basis of shift, splitting, and relative intensity ratio change of carboxylate bands. Conversely, öocyst surfaces comprise a complex mixture of interbonded macromolecules for which some of the absorbances may overlap in the infrared. Our approach to this added complexity is to examine spectral trends in response to well-controlled gradients in solution chemistry and thereby reveal the functional groups that are most affected by hematite surface interaction. Spectral shifts can then be interpreted in terms of the several excellent prior studies on model LMW carboxylic acids.

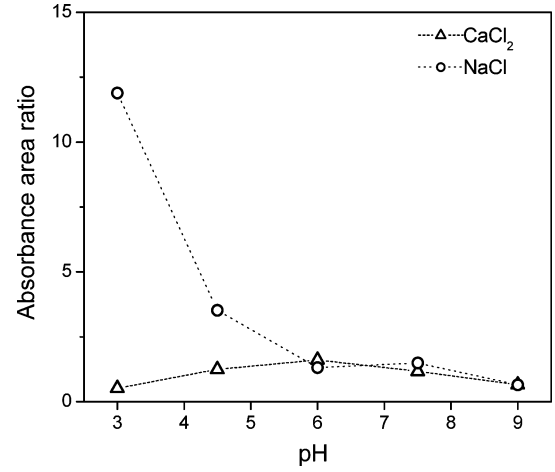

FIGURE 3. Intensity ratio of ν_s versus ν_{as} for COO^- stretching of spectra on a hematite surface as a function of pH.

Spectra of öocysts at pH 9 are useful for reference because cells and hematite are negative charged, and distinct differences were observed in carboxylate stretching bands with decreasing pH. A decrease in the intensity ratio of symmetric to asymmetric stretching vibration is observed with increasing pH in NaCl (Figure 3). Hwang et al. (*21*) also showed a pH dependency of this ratio, with the ratio increasing from pH 7.3 to 2.6 for carboxylic acids adsorbed to nanoparticulate α-Fe_2O_3. High values of the intensity ratio ν_s (COO^-) to ν_{as} (COO^-) are a diagnostic feature of inner-sphere complexation with mineral surface metal centers (*21, 26*). It is noteworthy that in a $CaCl_2$ solution, this ratio reaches a maximum at pH 6.0 (Figure 3).

Kinetics of Öocyst−Hematite Bonding. To assess the kinetics of an öocyst−hematite interaction as a function of solution chemistry, we focus on the symmetric carboxylate stretch, unaffected by the bending vibrations of H_2O. As we demonstrated in our previous paper, it takes ~3 min for öocysts to complete the physical setting process under the experimental conditions (*9*), while we observed that the IR signal takes a significantly longer time to reach the equilibrium. Such time dependence reflects the reorientation of

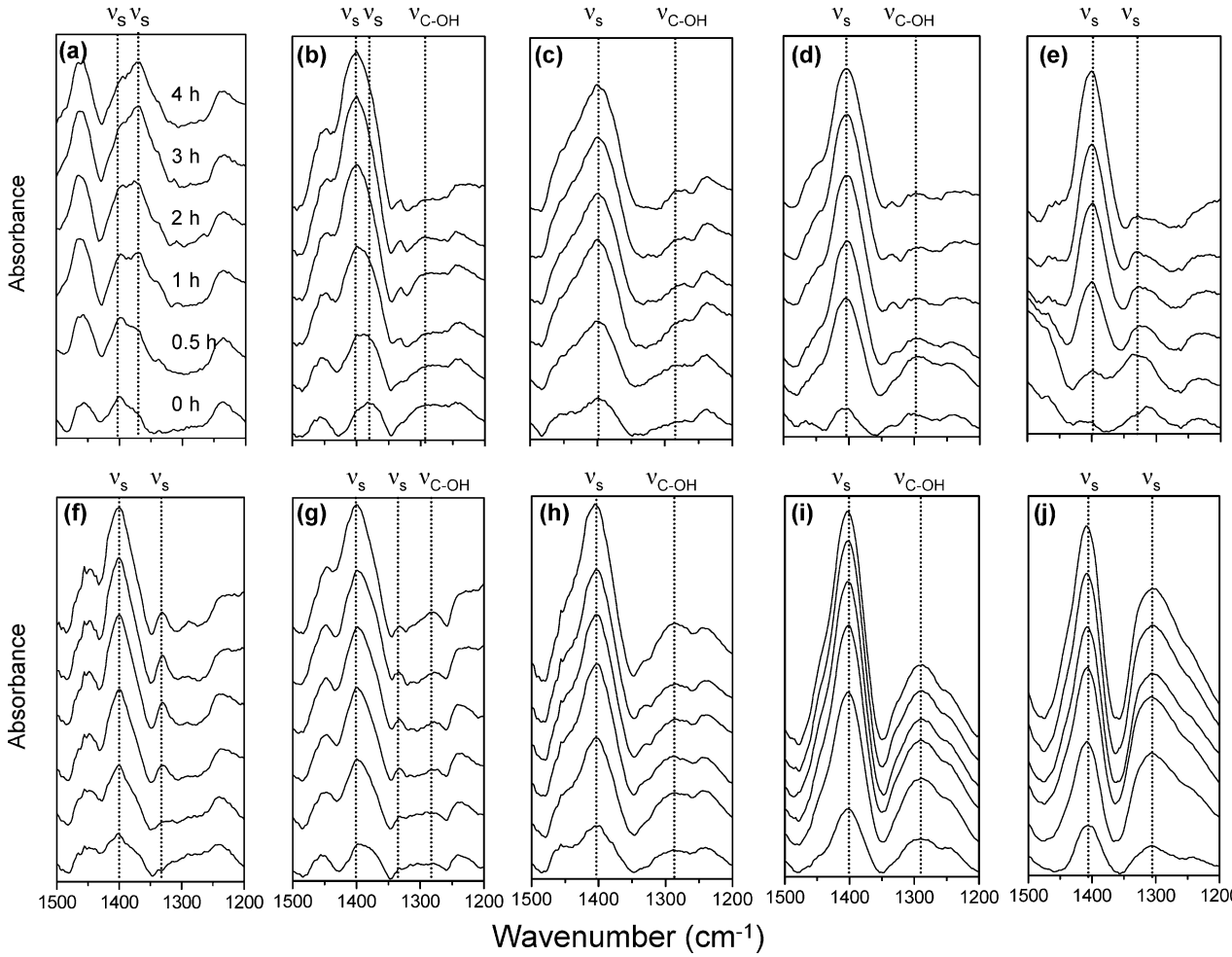

FIGURE 4. ATR-FTIR spectra of viable öocyst suspension on hematite surface as a function of time (0 min−4 h) in 10 mM NaCl solutions at (a) pH 3, (b) pH 4.5, (c) pH 6, (d) pH 7.5, and (e) pH 9, and 10 mM $CaCl_2$ solutions at (f) pH 3, (g) pH 4.5, (h) pH 6, (i) pH 7.5, and (j) pH 9.

biopolymers at the hematite−water interface, thereby providing kinetic information of the reaction. Panels a−e of Figure 4 show this spectral region (1500−1200 cm^{-1}) as a function of interaction time (0 min−4 h, proceeding from bottom to top) and pH (left to right) in 10 mM NaCl solution.

The separation in wavenumber ($\Delta\nu$) of ν_{as} and ν_s COO^- stretching bands can be used to elucidate bonding coordination and structure (*13, 22, 30*). In general, $\Delta\nu$ values greater than about 200 cm^{-1} are thought to indicate monodentate binding, whereas 180−150 cm^{-1} indicates binuclear bidentate (bridging) complexes, and <100 cm^{-1} indicates mononuclear bidentate binding (chelation) (*13, 22, 30, 31*). Because the asymmetric carboxylate stretch is subject to interference by amide II, we used the Grams/AI software to deconvolute the band and acquire the actual frequency of ν_{as} and ν_s COO^- (Figure S4 of the Supporting Information). At pH 3, the symmetric stretching of COO^- splits to two bands at 1400 and 1370 cm^{-1}, indicating the formation of additional complexes (Figure 4a). On the basis of the separation between ν_{as} and ν_s, if we attribute the peaks at 1400 cm^{-1} ($\Delta\nu$ = 177 cm^{-1}) and 1370 cm^{-1} ($\Delta\nu$ = 207 cm^{-1}) to binuclear bidentate and monodentate complexes, respectively, our results are consistent with the following interpretation. Initially, bidentate complexes are dominant, but the intensity of the peak assigned to the monodentate complex gradually increases with time and becomes the dominant complex mode at 4 h. However, this assignment of the 1400 cm^{-1} band to binuclear bidentate coordination is subject to uncertainty. We cannot, for example, rule out the possibility that this band arises from carboxylate binding to one Fe and also forming an H-bond with a hematite surface hydroxyl.

With increasing pH to 4.5, the relative intensity of ν_s COO^- is increased (Figure 4b). Early in the reaction, a broad peak at 1379 cm^{-1} and shoulder at 1400 cm^{-1} are consistent with two complex modes. The peak at 1379 cm^{-1} ($\Delta\nu \approx 200$ cm^{-1}) likely originates from a monodentate complex. A $\Delta\nu$ of 177 cm^{-1} for the shoulder at 1400 cm^{-1} suggests the presence of a binuclear bidentate complex. Progressive ingrowth of the 1400 cm^{-1} peak is consistent with the conversion of monodentate to a bidentate complex structure with increased reaction time. The relative intensity of the 1400 cm^{-1} band continues to increase with pH to 6.0 and 7.5 (Figure 4c,d). The single strong band at 1400 cm^{-1} suggests binuclear bidentate complexation as the principal bonding mechanism at pH 6 and 7.5. The same time dependencies were probed for the $CaCl_2$ background (Figure 4f−j). In contrast to the case for NaCl that seems to show two complexes at low pH (3 and 4.5), the spectra in $CaCl_2$ exhibit one strong band at 1400 cm^{-1} consistent with binuclear bidentate coordination.

Implications for Öocyst Transport in Soils and Aquifers. The fate and transport of öocysts in the subsurface environment are governed by interactions between öocyst cells and soil particles. These interactions include electrostatic and van der Waals interactions described by the DLVO theory and steric interactions generated from cell surface polymers. The spectroscopic data of öocysts adhesion to hematite provides direct evidence for the formation of Fe−carboxylate surface complexation at the mineral surface upon adhesion,

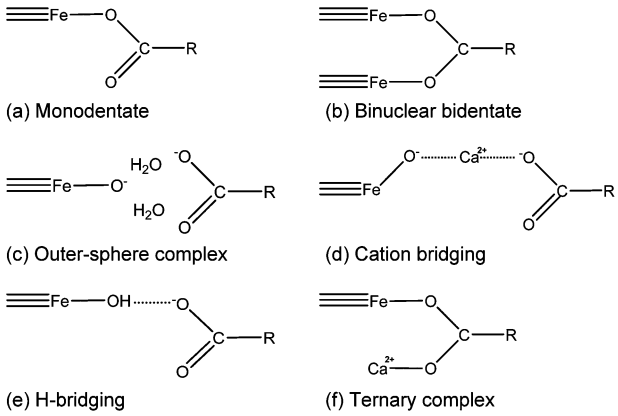

FIGURE 5. Schematic diagram of Fe−carboxylate complexes.

and such chemical bonds likely also mediate öocyst transport in the environment.

ATR-FTIR spectra indicate that molecular mechanisms of öocyst adhesion to hematite changes with solution chemistry. Specifically, öocysts form direct bonds to the hematite surface by inner-sphere Fe−carboxylate complexation at low pH (Figure 5a,b), whereas outer-sphere (electrostatic and cation-bridging) complexes occur at high pH (Figure 5c,d). These interactions are supplemented by H-bonding in the pH range of 4.5−7.5 (Figure 5e). This adhesion behavior is consistent with prior studies of ligand exchange at Fe oxide surfaces (*28*, *32*), which is less favorable at high pH when surface hydroxyls exhibit low proton surface charge. Conversely, at low pH, protonated hydroxyls exhibit higher lability and can be more readily exchanged for öocyst carboxylate groups for direct bonding to Fe metal centers (Figure S3 of the Supporting Information).

Background ion composition is also clearly important. In NaCl solution, öocysts are bound to the hematite surface via monodentate and binuclear bidentate complexes, whereas in $CaCl_2$, öocysts form only bidentate complexes. Ca^{2+} may form metal−ligand complexes with carboxylate in the aqueous phase, favoring carboxylate-metal−mineral ternary complexes (Figure 5f), which have similar symmetry to binuclear bidentate coordination (Figure 5b). Such ternary complexation may contribute to the binuclear bidentate assignments at low pH in $CaCl_2$ solution.

Abudalo et al. (*4*) studied the effects of Fe oxide coatings on the transport of öocysts in flow-through columns and reported increased öocyst attachment efficiency at low pH. They attributed this to a decrease in the electrostatic repulsive force between Fe oxides and cells. Our results suggest that, in addition to a decrease in the electrostatic force, direct bonding between the carboxylate groups and Fe (or Al) centers may also contribute significantly to high attachment efficiency at low pH. More generally, molecular-scale carboxylate−metal bonding likely modulates öocyst transport in soil and sediment environments.

Acknowledgments

This research was funded by the U.S. Department of Agriculture, National Research Initiative, Water and Watersheds Program (Grant 2006-35102-17192). Portions of this research were carried out at the Stanford Synchrotron Radiation Laboratory, a National User Facility operated by Stanford University on behalf of the U.S. Department of Energy, Office of Basic Energy Sciences.

Supporting Information Available

Infrared absorption band assignments for *C. parvum* öocysts, synchrotron XRD pattern, TEM micrograph, zeta potential of synthetic nanoparticulate hematite, and peak deconvolution of the öocyst spectra on hematite surface as a function of pH. The material is available free of charge via the Internet at http://pubs.acs.org.

Literature Cited

(1) Casemore, D. P.; Wright, S. E.; Coop, R. L. Cryptosporidiosis: Human and Animal Epidemiology, In *Cryptosporidium and Cryptosporidiosis*; Fayer, R. , Ed.; CRC Press: Boca Raton, FL, 1997; pp 65−92.

(2) Hsu, B. M.; Huang, C. P.; Pan, J. R. Filtration behaviors of *Giardia* and *Cryptosporidium*: Ionic strength and pH effects. *Water Res.* **2001**, *35*, 3777–3782.

(3) Considine, R. F.; Dixon, D. R.; Drummond, C. J. Öocysts of *Cryptosporidium parvum* and model sand surfaces in aqueous solutions: An atomic force microscope (AFM) study. *Water Res.* **2002**, *36*, 3421–3428.

(4) Abudalo, R. A.; Bogatsu, Y. G.; Ryan, J. N.; Harvey, R. W.; Metge, D. W.; Elimelech, M. Effect of ferric oxyhydroxide grain coatings on the transport of bacteriophage PRD1 and *Cryptosporidium parvum* öocysts in saturated porous media. *Environ. Sci. Technol.* **2005**, *39*, 6412–6419.

(5) Kuznar, Z. A.; Elimelech, M. Adhesion kinetics of viable *Cryptosporidium parvum* öocysts to quartz surfaces. *Environ. Sci. Technol.* **2004**, *38*, 6839–6845.

(6) Kuznar, Z. A.; Elimelech, M. Role of surface proteins in the deposition kinetics of *Cryptosporidium parvum* öocysts. *Langmuir* **2005**, *21*, 710–716.

(7) Kuznar, Z. A.; Elimelech, M. Cryptosporidium öocyst surface macromolecules significantly hinder öocysts attachment. *Environ. Sci. Technol.* **2006**, *40*, 1837–1842.

(8) Tufenkji, N.; Elimelech, M. Spatial distributions of *Cryptosporidium* öocysts in porous media: Evidence for dual mode deposition. *Environ. Sci. Technol.* **2005**, *39*, 3620–3629.

(9) Gao, X.; Chorover, J. In situ monitoring of *Cryptosporidium parvum* öocyst surface adhesion using ATR-FTIR spectroscopy. *Colloids Surf., B.* **2009**, *71*, 169–176.

(10) Omoike, A.; Chorover, J.; Kwon, K. D; Kubicki, J. D. Adhesion of bacterial exopolymers to α-FeOOH: Inner-sphere complexation of phosphodiester groups. *Langmuir* **2004**, *20*, 11108–11114.

(11) Omoike, A.; Chorover, J. Adsorption to goethite of extracellular polymeric substances from Bacillus subtilis. *Geochim. Cosmochim. Acta.* **2006**, *70*, 827–838.

(12) Parikh, S. J.; Chorover, J. ATR-FTIR spectroscopy reveals bond formation during bacterial adhesion to iron oxide. *Langmuir* **2006**, *22*, 8492–8500.

(13) Ojeda, J. J.; Romero-Gonzalez, M. E.; Purran, H. M.; Banwart, S. A. In situ monitoring of the biofilm formation of *Pseudomonas putida* on hematite using flow-cell ATR-FTIR spectroscopy to investigate the formation of inner-sphere bonds between the bacteria and the mineral. *Mineral. Mag.* **2008**, *72*, 101–106.

(14) Sposito, G. *The Chemistry of Soils*; Oxford University Press: New York, 1989.

(15) Bolster, C. H.; Mills, A. L.; Hornberger, G. M.; Herman, J. S. Effect of surface coatings, grain size, and ionic strength on the maximum attainable coverage of bacteria on sand surfaces. *J. Contam. Hydrol.* **2001**, *50*, 287–305.

(16) Mills, A. L.; Herman, J. S.; Hornberger, G. M.; Dejesus, T. H. Effect of solution ionic strength and iron coatings on mineral grains on the sorption of bacterial cells to quartz sand. *Appl. Environ. Microbiol.* **1994**, *60*, 3300–3306.

(17) Ha, J. Y.; Yoon, T. H.; Wang, Y. G.; Musgrave, C. B.; Brown, G. E. Adsorption of organic matter at mineral/water interfaces: 7. ATR-FTIR and quantum chemical study of lactate interactions with hematite nanoparticles. *Langmuir* **2008**, *24*, 6683–6692.

(18) Jiang, W; Saxena, A.; Song, B.; Ward, B. B.; Beveridge, T. J.; Myneni, S. C. B. Elucidation of functional groups on gram-positive and gram-negative bacterial surfaces using infrared spectroscopy. *Langmuir* **2004**, *20*, 11433–11442.

(19) Schwertmann, U.; Cornell, R. M. *Iron oxides in the Laboratory: Preparation and Characterization*; Wiley-VCH: Weinheim, Germany, 1991.

(20) Duckworth, O. W.; Martin, S. T. Surface complexation and dissolution of hematite by C_1−C_6 dicarboxylic acids at pH 5.0. *Geochim. Cosmochim. Acta* **2001**, *65*, 4289–4301.

(21) Hwang, Y. S.; Liu, J.; Lenhart, J. J.; Hadad, C. M. Surface complexes of phthalic acid at the hematite/water interface. *J. Colloid Interface Sci.* **2007**, *307*, 124–134.

(22) Dobson, K. D.; McQuillan, A. J. In situ infrared spectroscopic analysis of the adsorption of aliphatic carboxylic acids to TiO_2, ZrO_2, Al_2O_3, and Ta_2O_5 from aqueous solutions. *Spectrochim. Acta,Part A.* **1999**, *55*, 1395–1405.

(23) Nordin, J.; Persson, P; Laiti, E.; Sjoberg, S. Adsorption of *o*-phthalate at the water−boehmite (γ-AlOOH) interface: Evidence for two coordination modes. *Langmuir* **1999**, *13*, 4085–4093.
(24) Smith, R. M.; Martell, A. E. *Critical Stability Constants*. Plenum Press: New York, 1976.
(25) Hwang, Y. S.; Lenhart, J. J. Adsorption of C4-dicarboxylic acids at the hematite/water interface. *Langmuir* **2008**, *24*, 13934–13943.
(26) Yoon, T. H.; Johnson, S. B.; Musgrave, C. B.; Brown, G. E. Adsorption of organic matter at mineral/water interfaces: I. ATR-FTIR spectroscopic and quantum chemical study of oxalate adsorbed at boehmite/water and corundum/water interfaces. *Geochim. Cosmochim. Acta* **2004**, *68*, 4505–4518.
(27) Awatani, T.; Dobson, K. D.; McQuillan, A. J.; Ohtani, B.; Uosaki, K. In situ infrared spectroscopic studies of adsorption of lactic acid and related compounds on the TiO_2 and CdS semiconductor photocatalyst surfaces from aqueous solutions. *Chem. Lett.* **1998**, *8*, 849–850.
(28) Peak, D.; For, R. G.; Sparks, D. L. An in situ ATR-FTIR investigation of sulfate bonding mechanisms on goethite. *J. Colloid Interface Sci.* **1999**, *218*, 289–299.
(29) Parikh, S. J.; Chorover, J. ATR-FTIR study of lipopolysaccharides at mineral surfaces. *Colloids Surf., B.* **2008**, *62*, 188–198.
(30) Chu, H. A.; Hillier, W.; Debus, R. J. Evidence that the C-terminus of the D1 polypeptide of photosystem II is ligated to the manganese ion that undergoes oxidation during the S1 to S2 transition: An isotope-edited FTIR study. *Biochem.* **2004**, *43*, 3152–3166.
(31) Deacon, G. B.; Phillips, R. Relationships between the carbon−oxygen stretching frequencies of carboxylato complexes and the type of carboxylate coordination. *Coord. Chem. Rev.* **1980**, *33*, 227–250.
(32) Hug, S. J. In suit Fourier transform measurements of sulfate adsorption on hematite in aqueous solutions. *J. Colloid Interface Sci.* **1997**, *188*, 415–422.

ES901346Z